OPEN ACCESS

University of BRISTOL

Eckstein, E. N., Weaver, P. M., & Halbig, M. C. (2016). Thermally-driven morphing with high temperature composites. In 57th AIAA/ASCE/AHS/ASC Structures, Structural Dynamics, and Materials Conference. [AIAA 2016-1241] American Institute of Aeronautics and Astronautics Inc, AIAA. 10.2514/6.2016-1241

Peer reviewed version

Link to published version (if available):
10.2514/6.2016-1241

Link to publication record in Explore Bristol Research
PDF-document

University of Bristol - Explore Bristol Research

General rights

This document is made available in accordance with publisher policies. Please cite only the published version using the reference above. Full terms of use are available:
http://www.bristol.ac.uk/pure/about/ebr-terms.html

Take down policy

Explore Bristol Research is a digital archive and the intention is that deposited content should not be removed. However, if you believe that this version of the work breaches copyright law please contact open-access@bristol.ac.uk and include the following information in your message:

• Your contact details
• Bibliographic details for the item, including a URL
• An outline of the nature of the complaint

On receipt of your message the Open Access Team will immediately investigate your claim, make an initial judgement of the validity of the claim and, where appropriate, withdraw the item in question from public view.

Thermally-Driven Morphing with High Temperature Composites

Eric Eckstein * and Paul M Weaver†

University of Bristol, Department of Aerospace Engineering. Bristol, BS8 1TR, United Kingdom

Michael C Halbig‡

NASA Glenn Research Center, Cleveland, OH 44135

The thermal expansion mismatch between heat-resisting metals and high-temperature composite materials is explored as a method of achieving thermally-driven morphing in elevated-temperature environments, with an eye towards applications in variable-geometry hot structures in gas turbine engines. Three concepts are presented and demonstrated. The first thermal morphing system is a bimorph laminate which exploits the CTE mismatch between a titanium metal matrix composite and its parent titanium matrix material. The second concept is similar to the first, but uses a diffusion-bonded austenitic stainless steel alloy as the high expansion layer. The third concept utilizes a carbon fiber, silicon carbide matrix ceramic matrix composite joined to a stainless steel skin in a trailing-edge flap arrangement. Furnace-based experiments of cantilever-mounted specimens are performed to evaluate the displacement response of the metal-matrix and ceramic-matrix concepts at temperatures up to 606°C and 1035°C, respectively.

Nomenclature

MMC	Metal matrix composite
CMC	Ceramic matrix composite
CLT	Classical laminate theory
κ	Curvature
w_{rel}	Relative transverse displacement

*PhD Student, Advanced Composites Centre for Innovation and Science, AIAA student member

†Professor in Lightweight Structures, Advanced Composites Centre for Innovation and Science, AIAA member

‡Materials Research Engineer, NASA GRC Ceramics Branch, AIAA non-member.

I. Introduction

I.A. Research Motivation

Variable geometry structures have been identified as a technology which can enable performance improvements in gas turbine aero-propulsion applications.[1,2] Conventionally, variable geometry has been achieved using electromechanical or hydraulic linear actuators acting upon mechanisms of linkages, bearings, and hinges. Examples of such include variable geometry inlet guide vanes and afterburner exhaust nozzles, as shown in Figure 1. This conventional approach has so far been restricted to applications outside the engine combustor and turbine sections on account of the challenges presented by such a hot and corrosive environment. In particular, variable geometry mechanisms are challenged by large temperature excursions, which present difficulties in maintaining close tolerances while avoiding seizure or galling. Meanwhile, current hydraulic and servo-electric actuators are limited to relatively low temperatures, and thus restricted to locations outside the engine core.

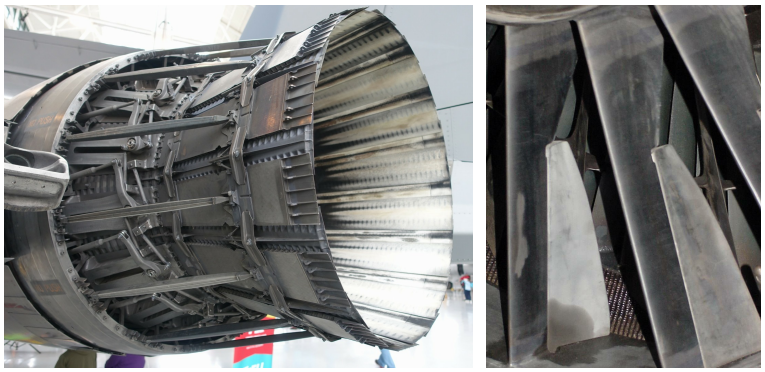

Figure 1. Two examples of the mechanism approach towards variable geometry gas turbine components. Pratt & Whitney F100 variable exhaust nozzle, and Pratt & Whitney J58 variable inlet guide vane (silver blade), which pivots aft of the black-colored static guide vane.

Morphing structures, that is, structures which displace via smooth, typically elastic deformations, may present a viable alternative to the conventional mechanism-based strategies. A flexural hinge, for example, is free from the lubrication requirements of a conventional hinge, does not develop free-play, nor is susceptible to thermally or chemically-induced seizure. In addition, the smooth-deformation nature of morphing structures is generally more advantageous than rigid body rotations or displacements for applications in aerodynamic surfaces.

A morphing-based strategy may also allow mechanically simple solutions to the high-temperature actuation problem. Strain-based actuation concepts such as shape memory alloys, piezoelectrics, and thermal-expansion driven systems present the opportunity to combine actuator and structure into one, a trait which may be particularly beneficial in applications where packaging of traditional actuation systems would be impractical. This feature is well exemplified by active turbine tip clearance control, a thermal expansion-based technology employed on most modern civil turbofans.[3] While much progress has been made towards improving the high-temperature properties of shape memory alloys (SMAs) and piezoelectrics, this study focuses on evaluating the feasibility and flexural performance of thermal expansion-based systems. Given a sufficient temperature change, these sorts of systems are competitive with SMAs in terms of specific actuation performance.[4] The most appealing use of thermal morphing systems may lie in passive shape control of gas turbine components, some examples are given in Figure 2. As long as the desired shape of combustor, nozzle vane, etc at each operating condition can be correlated to a unique gas temperature at that condition, a thermal morphing structure can adapt its shape in a purely passive manner. Specific applications may include variable control of cooling flow, combustor dilution, nozzle vane geometry, and core exhaust chevron geometry.

The present study is concerned with two structural concepts: The simple bimorph laminate, as well as a flap-like section consisting of two skins joined at their trailing edge.

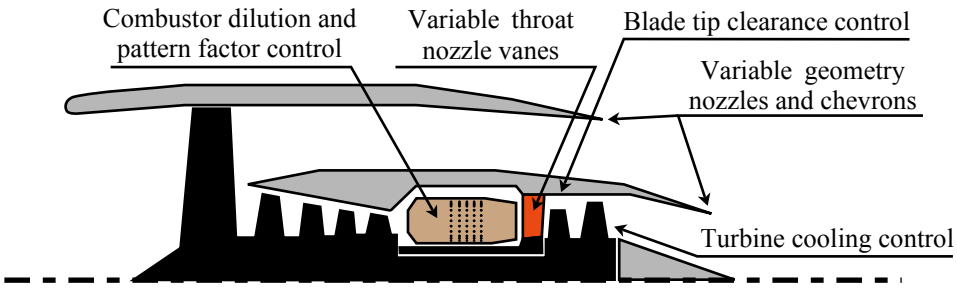

Figure 2. Potential gas-turbine applications of thermally-driven morphing structures.

I.B. Thermally-driven Bimorphs

Thermal bimorphs are laminated structures fabricated from at least two or more joined layers with mismatched thermal expansion coefficients (CTE), which respond to temperature change with generation of thermal stresses. These stresses act eccentrically about the laminate's neutral axes, thus generating internal bending moments in one or more directions. These bending moments resolve themselves as curvatures, subject to any external forces or geometric constraints. The first thermal bimorphs were developed by eighteenth-century clockmaker John Harrison in order to improve the timekeeping accuracy of marine chronometers.[5] They have since found use in applications ranging from thermostats[6] to spacecraft thermal control systems.[7]

Classically, thermal bimorphs are constructed from two metals,[6,8] whose isotropic properties lead to internal moments which are equal in all directions. This isotropy has the effect of limiting the acceptable range of geometries available to the designer, as the preferred direction of bending becomes coupled to geometry and boundary conditions.[9] The use of composite materials opens the possibility to create thermal bimorphs which are anisotropic in terms of both stiffness and thermal moments. The direct result is that bimorphs may be created which exhibit bending action in a direction determined by material orientations rather than geometry, thus allowing the designer freedom to specify general planform geometries. In addition, composites generally have very low CTEs on account of the low longitudinal CTE of their fibers. In the case of carbon and other ceramic fibers, this low CTE is maintained even at very high temperatures, which allows a large CTE mismatch between layers to be obtained across a wide range of temperatures.

Some of the unique properties of composite bimorphs have been demonstrated using polymer-matrix bimorphs,[10] however as our goal is to attain thermal morphing at high temperatures, we need to turn to more exotic materials. Asanuma et al. showed that the CTE mismatch between silicon carbide fibers and a nickel alloy could be used to produce curvature in thin laminates.[11] We expand up this concept with developments in thermal bimorphs constructed from both metal matrix and ceramic matrix composites.

I.C. Thermal Morphing with Flap-Section Geometry

The bimorph is perhaps the simplist method of generating large displacements from relatively small strains, but as it is a solid-core laminate (i.e. not hollow or sandwich construction), it has relatively poor bending stiffness for its weight. By separating the high and low-expansion skins, a higher specific bending stiffness can be attained, albeit at the cost of displacement amplitude. This concept has been previously investigated for variable-geometry nozzle chevrons, using an SMA skin joined to an opposing titanium skin.[12] We aim to implement a similar concept which exploits the large thermal expansion mismatch between austenitic stainless steel and a ceramic matrix composite.

II. Materials and Manufacturing

II.A. Metal Matrix Composite Bimorphs

Two types of MMC bimorphs were fabricated for this study, both produced by TISICS, Inc (Farnborough, UK). A summary of the manufacturing process and parameters is given in Figure 3 and Table 1, respectively.

II.A.1. MMC-Ti Bimorph

The first bimorph type is a laminate in which the low-expansion layer is constructed from a unidirectionally reinforced titanium-matrix composite, and the high-expansion layer is of monolithic titanium alloy. The reinforcing fibers are SM3156 silicon carbide (SiC) monofilaments, which are produced in-house by TISICS via chemical vapor deposition of SiC on a tungsten filament. Both the composite matrix and monolithic layer is commercially available Ti-3Al-2.5V alloy. The MMC layer was laid up by stacking alternate layers of 140μm titanium foils and binder-bound SiC monofilaments, while the monolithic layer comprises the same titanium foils stacked to the required layer thickness. The complete layup was encapsulated in a welded stainless steel canister in preparation for consolidation. The binder was vaporized, followed by evacuation and sealing of the canister. Consolidation was achieved by hot isostatic pressing (HIP). The exact HIP cycle parameters are propitiatory to TISICS, however publicly available literature indicates that a chamber pressure of 70-90 MPa, temperature of 900°C, and and hold time of 30 minutes is typical for this material system.[13] After completion of the HIP cycle, the compacted canister was cut open and the consolidated laminates extracted and cut into 0° and 90° fiber-orientation specimens by wire electro-discharge machining.

Specimens were mounted in epoxy and polished for micrograph analysis. The consolidated MMC-Ti bimorph laminates showed generally uniform fiber distribution and were free of voids, as shown in Figure 4.

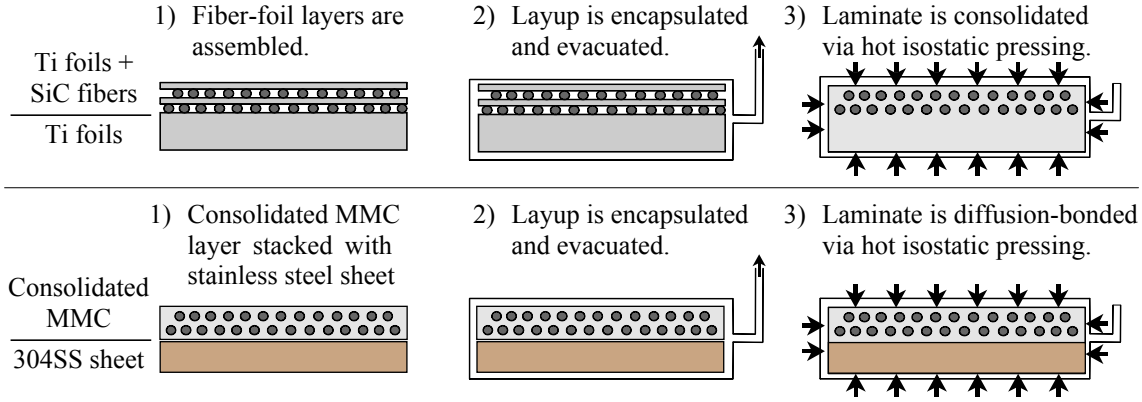

Figure 3. Manufacturing process used to create the MMC-Ti bimorphs (top) and MMC-304SS bimorphs (bottom) .

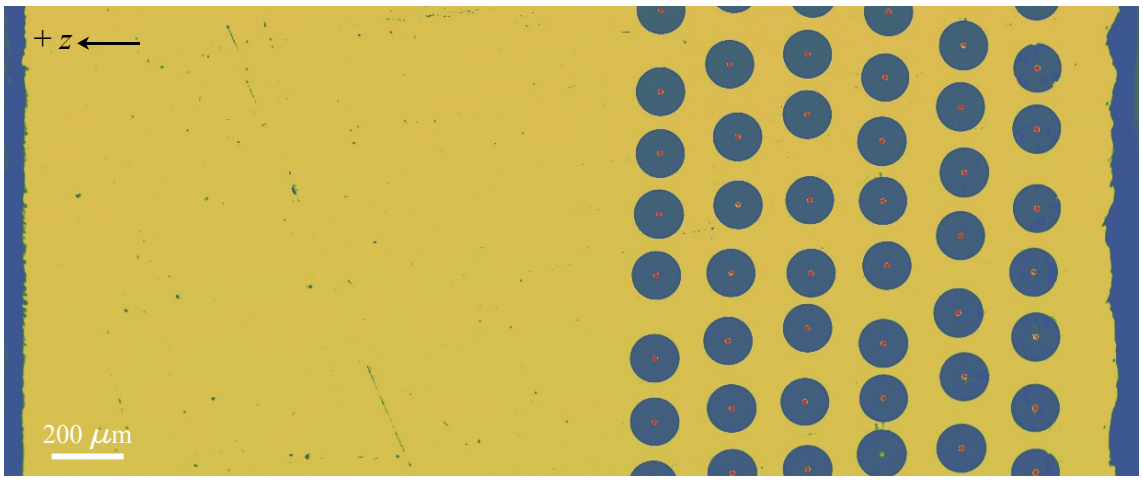

Figure 4. False-color SEM micrograph of MMC-Ti laminate cross-section. Note that the image is perpendicularly oriented to the sketches in Figure 3.

II.A.2. MMC-304SS Bimorph

The second type of MMC bimorph features the same low-expansion MMC layer as the first, while the high expansion layer is a 1.6mm sheet of AISI 304 stainless steel. This material choice was motivated by the higher displacements and moments achievable by increasing the CTE mismatch between layers. Austenitic

Table 1. Manufacturing specifications for MMC bimorphs.

Test Article Name:	MMC-Ti 0°	MMC-Ti 90°	MMC-304SS 0°	MMC-304SS 90°
Layup: Ti = Ti-3Al-2V foil SiC($x°$) = SiC fiber ply oriented at at $x°$ SS = 304SS sheet	[Ti_{13}/ ($SiC(0°)/Ti)_6$]	[Ti_{13}/ ($SiC(90°)/Ti)_6$]	[SS_1/Ti_1/ ($SiC(0°)/Ti)_6$]	[SS_1/Ti_1/ ($SiC(90°)/Ti)_6$]
Planform [mm]	90 x 10	90 x 10	90 x 10	90 x 10
Composite layer total thickness [mm]	1.48	1.48	1.61	1.61
Monolithic layer total thickness [mm]	1.67	1.67	1.44	1.44

stainless steels provide the highest CTE of practical engineering metals, and thus the MMC-304SS bimorph possesses a CTE mismatch approximately 3.6 times greater than the MMC-Ti bimorph in the fiber direction.

Interlaminar peel stresses scale with CTE mismatch at the interface, consequently these deleterious stresses can be reduced by inserting an interlayer material with an intermediate CTE.[14] To that end, an additional 140μm titanium foil was inserted between the MMC and 304SS layers in order to reduce the likelihood of delamination due to bond-line peel stresses.

The laminate was constructed in two HIP cycles. The first cycle consolidates the MMC layer alone using the same HIP cycle as the MMC-Ti bimorph, while the second HIP cycle diffusion bonds the stainless steel layer to the consolidated MMC using the same cycle parameters again, apart from a lower temperature of 850°C.[a]

The resulting MMC-304SS laminates exhibited consistent fiber spacing and void-free bond line, as shown in Figure 5. An energy-dispersive X-ray (EDX) analysis was carried out in order to determine the composition of the diffusion-bonded interfacial layer. The results, shown in Figure 6, indicate that the interfacial layer comprises Fe-Ti solid solutions and intermetallic compounds. EDX analysis has limited ability to determine the types of intermetallic compounds present, however prior literature suggests that the main constituent compounds are brittle FeTi and Fe_2Ti intermetallics. This brittle layer did not give us any trouble in the course of our experiments, though we do note that prior workers have addressed the brittle interface problem through use of a copper interlayer, which also functions as both a diffusion barrier and a ductile interface.[16]

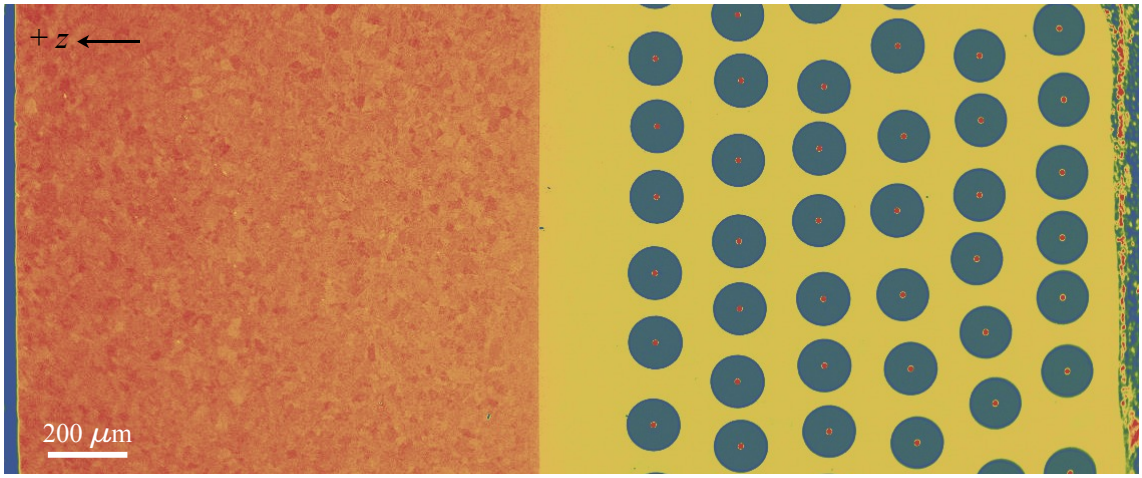

Figure 5. False-color SEM micrograph of MMC-304SS laminate cross-section.

[a]We also attempted to consolidate and diffusion bond the entire laminate in a single HIP cycle, however this resulted in partial debonding between the MMC and stainless steel layers. Energy dispersive X-ray analysis as well as previous literature[15] suggests the $\sim$ 50°C higher HIP temperature needed to achieve complete composite consolidation, compared to diffusion bonding, resulted in a degradation of bond strength on account of excessive Fe-Ti intermetallic formation at the bond line.

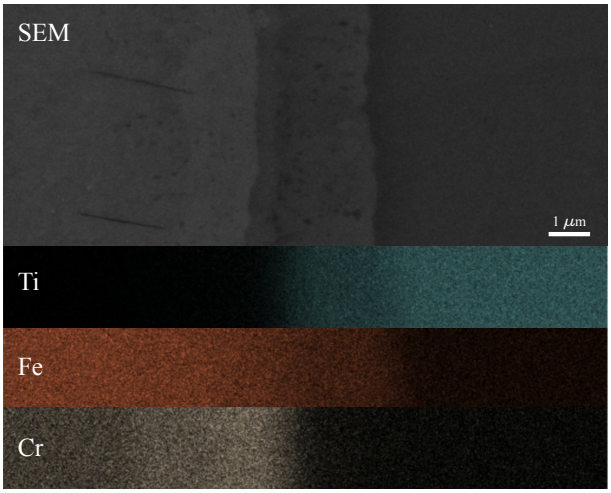

Figure 6. SEM micrograph and overlaid EDX K-shell emission densities of the MMC-304SS diffusion-bonded interface, showing a void-free bond with a reaction layer of Fe-Ti compounds. Other major alloying elements were not present in significant concentrations in the reaction layer.

Table 2. Thermoelastic material properties for the composites and metals used in this study. Properties are given at room temperature unless otherwise stated.

	E_1 or E [GPa]	E_2 [GPa]	α_1 or α $[\frac{10^{-6}}{^\circ C}]$	α_2 $[\frac{10^{-6}}{^\circ C}]$
SiC/Ti-3Al-2.5V MMC[17,18]	205	150	6.6 (0-700°C)	9.3 (0-700°C)
Ti-3Al-2.5V[19,20]	100		9.6 (0-100°C)	
	80 (230°C)		10.0 (0-540°C)	
	55 (500°C)			
AISI Type 304 SS[20]	195		17.1 (0-200°C)	
	127 (800°C)		19.4 (0-800°C)	
AISI Type 310 SS[21]	200		16.2 (0-315°C)	
			17.0 (0-538°C)	
C/SiC CMC[22]	67.4 (flexural test by authors)	N/A	2 (0-1000°C)	5 (0-1000°C)

II.B. Hybrid CMC-Metallic Bimorphs

Our proposed metallic-CMC bimorph concept aimed to exploit the high-temperature strength and high CTE mismatch between ceramic matrix composites and metallic alloys. The basic procedure involved brazing a low CTE ceramic composite layer to a relatively high CTE nickel superalloy. Ultimately, this effort failed to yield robust CMC-metallic bimorphs, however the CMC material fabricated for this effort was ultimately used in the flap-section morphing device presented in Section II.C. Nonetheless, a summary covering procedures and results is given for the benefit of future research efforts.

II.B.1. CMC Manufacturing

Carbon fiber, silicon carbide matrix (C/SiC) CMC laminates were manufactured in-house at the University of Bristol using the polymer infiltration and pyrolysis (PIP) method. The laminate comprises four central plies of 0° UD IM7 carbon non-crimp fabric, capped on each side by a single ply of ±45° 5-harness satin weave T300 carbon fabric.[b] Both carbon fabrics were de-sized and chemical vapor coated with a pyrolytic carbon (PyC) layer of 0.7μm average thickness (Archer Technicoat, High Wycombe, UK).

The dry fabric stack was slurry-infiltrated at ambient temperature and pressure via a wet layup. The slurry consisted of 25 wt% 6μm SiC powder and 1 wt% dicumyl peroxide catalyst suspended in SMP-10 Allylhydridopolycarbosilane (AHPCS) SiC-forming polymer (Starfire Systems, Schenectady, NY). This fraction of SiC powder filler was found to reduce matrix porosity without jeopardizing the polymer's infiltration performance, as corroborated in other literature.[23,24]

The slurry-infiltrated fabric was hot-pressed on a flat tool at 220°C under 515 kPa of pressure for 1 hour, yielding solidified polymer-matrix green bodies. These were was subsequently heated under argon atmosphere to 900°C in a retort furnace, thus converting the preceramic polymer matrix to a SiC matrix. The pyrolysis of AHPCS to SiC is accompanied by significant shrinkage, resulting in a porous matrix. As is normal for the PIP process, this porosity was reduced by repeated vacuum-infiltration and pyrolysis of additional AHPCS. A total of 11 infiltration-pyrolysis cycles yielded an average open porosity of 6.1%, determined by the mass of polymer uptake on the final infiltration cycle. Total porosity, which cannot be measured by this method, was unknown, however analysis of sectional micrographs indicates an average porosity of roughly 15%. The densified laminates were cut into strips using a diamond saw. The strength of the laminate was evaluated by 3-point flexural testing, resulting in an average flexural strength of 275 MPa.

II.B.2. CMC-Metallic Bimorph Joining

Along with manufacturing the CMC laminate, the chief challenge in fabricating CMC-metallic bimorphs lies in joining the metallic and composite layers in a manner suitable for high-temperature applications. Currently, ceramic composites and metals may be joined in such a manner using a process known as active metal brazing. Conventional braze alloys have difficulty wetting ceramic surfaces. In contrast, active metal brazes contain a small proportion of a carbide-forming metal, typically titanium, in order to promote reaction and wetting of the ceramic surface.

CMC-metal brazing trials were conducted at NASA Glenn Research Center, Cleveland OH. Cusil-ABA braze paste (Morgan Advanced Ceramics, Hayward, CA) was trialed for joining the University of Bristol CMC to Incoloy 800H coupons of 3.2 mm thickness. The paste was applied using a spatula to the surfaces of the CMC and Incoloy 800H substrates that were to be paired for joining. The assembly was loaded with a normal pressure of 0.2–0.4MPa using dead weight, and heated in a vacuum furnace to 830°C. The samples were isothermally held for 5 minutes, and slowly cooled to room temperature at a controlled rate, ~ 5°C per minute down to 500° C, followed by free convective cooling under nitrogen atmosphere. The joined samples were mounted in epoxy and polished in preparation for metallurgical examination.

The joint region was analyzed using SEM and EDX techniques, with a well-bonded region shown in Figure 7. Despite a bondline that appeared continuous to the naked eye, microscopy revealed significant regions of debonding, with the failure occurring within the predominately-SiC outer layer of the CMC.

Prior theoretical analysis of ceramic-metal joints indicates that stresses in the ceramic layer are reduced with the thickness of the metal layer is reduced,[25] and when the CTE mismatch between layers is minimized. To that end, coupon trials were undertaken using Inconel 625 alloy of varying thickness between 0.8-3.0 mm.

[b] We also attempted to fabricate a completely UD laminate, however the resulting composite had inconsistent dimensional stability.

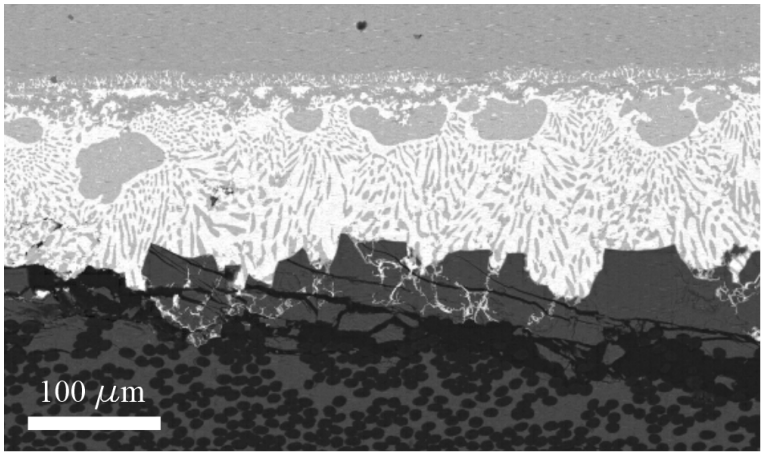

Figure 7. SEM micrograph of C/SiC CMC (bottom) and Incoloy 800H (top) joined with a fully-wetted brazed interface. The horizontal cracks visible in the outer SiC matrix layer were the site of debonding in failed specimens. The leopard-spot pattern in the braze layer is eutectic layering of the Cu-Ag braze.

Inconel 625 is a nickel-based superalloy with a CTE approximately 20% less than Incoloy 800H, and thus we hoped to achieve a successful bond without compromising high-temperature material properties.

Using identical braze cycle parameters as described previously, we found that when using our thinnest gauge metal (0.8 mm), small coupon specimens of roughly 35 mm length could successfully be joined without gross interfacial debonding, as shown in Figure 8. However, longer coupons or those using thicker gauges exhibited total debonding as also shown in Figure 8. The length effect may be related to the fact that interfacial shear stresses increase with longer bond lengths.[14] However as the stress-relief effect ris only significant for bond lengths less than roughly ten times the thickness of the laminate. Our laminates had a minimum length of of roughly nine times their thickness. An alternative possibility is that larger laminates simply present a greater probability of containing a flaw in the braze joint of size greater than the critical crack length for the material.

Historically, successful CMC-metal brazing has been achieved by making efforts to reduce thermal mismatch stresses.[26] This runs counter to the typical bimorph strategy of maximizing mismatch stresses, however it is possible that a successful solution may lie in compromising bimorph actuation performance in favor of durability, perhaps through the use of an intermediate CTE interlayer. At the present time however, the effort has yet to be successful on a practical scale.

Figure 8. Photograph of debonded braze interface (left) and successfully joined laminate (right). Note the curvature that has developed in the joined laminate.

II.C. CMC-Metallic Flap Section

Although a bimorph laminate is perhaps the most structurally simple method of converting thermal strains into large displacements, other concepts exist, particularly those which do not require complete and continuous joining of the low and high expansion layers. One such concept consists of a pair of skins, fastened to a root and joined along a common edge in a flap-like arrangement as shown in Figure 9. In this concept, differential thermal expansion still acts to produce transverse displacement, however unlike the bimorph, the curvatures generated are non-constant across the chord.

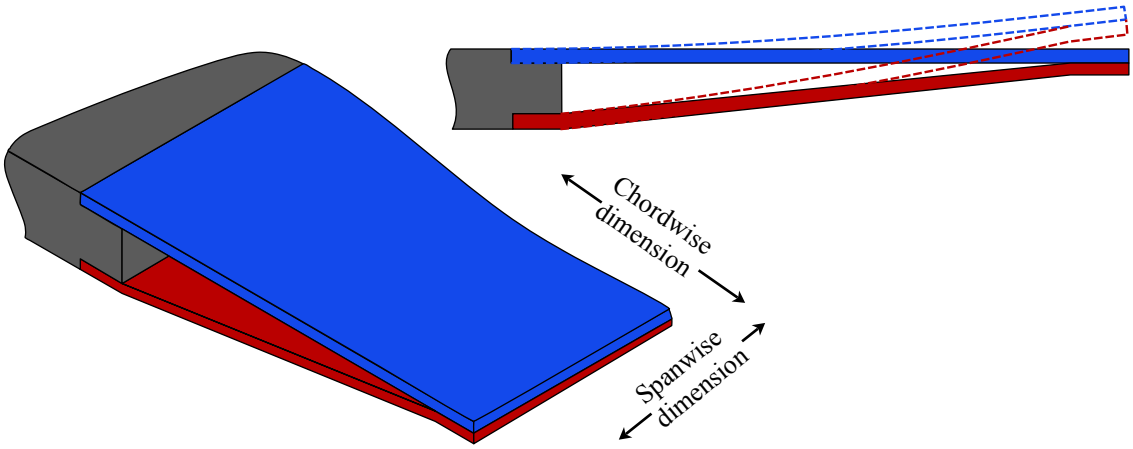

Figure 9. Drawing of the flap section thermal actuator concept. Dotted outlines show the approximate displacement field upon heating, assuming the red surface has a higher CTE than the blue.

Due to our lack of success in manufacturing a CMC-metallic bimorph, we turn our attention to this flap-section concept as a method to achieve thermally-driven morphing at high temperatures. The low expansion element is constructed from the same C/SiC laminate described in Section II.B.1, while the high expansion element is fabricated from a 1.5mm thick sheet of AISI 310 stainless steel, a high-nickel austenitic alloy. Our manufactured flap segments are relatively narrow, having a span of 20 mm for chord of 80 mm. While this beam-like geometry has the disadvantage of hindering observation of spanwise curvature and its effects, it was necessary due to the size limitations of our furnace. As shown in Figure 10, the two elements are joined to each-other using a pair of 3.2 mm pop-rivets, and mounted to a test fixture using a single M6 fastener. All fasteners and fixtures are of 304 stainless steel.

Table 3. Manufacturing specifications for CMC-metallic flap sections.

Composite layup wv = woven T300 ud = unidirectional IM7	$[45_1^{wv}/0_2^{ud}]_s$
Chord x span [mm]	80 x 20
CMC layer thickness [mm]	2.85
310SS layer thickness [mm]	1.50
Total section thickness at root [mm]	14.2

III. Experimental Procedures

The goal of our experiment is to measure the thermally-induced displacements of the presently studied structures, as well as determine the approximate temperature at which each structure's thermal response fails to be repeatable. Our experiment uses an optical target-tracking system to determine the displacement of painted-on targets. These targets are black dots located at the root and tip of each of our test articles, shown in Figure 10 . The figure also shows the 304 stainless steel fixture to which the test articles are bolted.

Our experimental setup is shown in Figure 11. The test fixture assembly is placed in an electrically-heated furnace, where it is viewed side-on by a thermal still camera (FLIR Systems, Wilsonville, OR) and an optical video camera (Imetrum, Bristol, United Kingdom). The furnace door is kept closed while it heats and stabilizes at the desired measurement temperature. After a 30 minute hold to allow the test fixture and test articles to thermally equilibrate, the furnace door is opened for approximately 10 seconds, during which the optical and thermal cameras capture imagery. Displacements are extracted from video data using Imetrum VideoGauge software.

Being a somewhat unconventional high-temperature test technique, some problems had to be overcome. First, opening the door introduces a draft of cold air into the furnace, however our displacement data showed that the effect of this draft was negligible for roughly the first four seconds after door opening. Thus, our

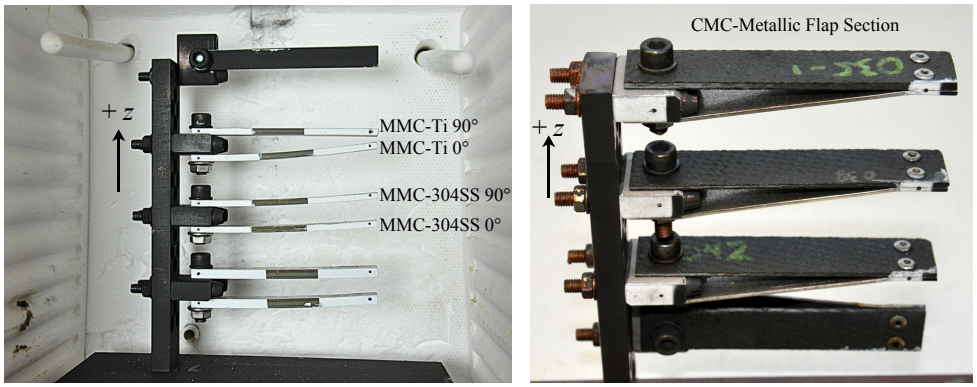

Figure 10. MMC bimorph (left) and CMC-metallic flap-section (right) test articles mounted on the test fixture with tracking targets painted on. In each image, one test article is turned 90° relative to the others in order to provide the thermal camera with a face-on view, thus providing a representative assessment of the temperature uniformity of the test articles. The lowest two test articles on each photo used alternate laminates and joining methods, their results are not presented in this work.

displacements are determined from the first two seconds of video.

In addition, the mixing of cold and hot air causes a small degree of shimmering in the video data, in the same sense that the horizon over an asphalt road appears to shimmer on a sunny day. We found that despite this shimmering, consistent displacements could still be recorded by averaging the results of several consecutive video frames. This consistency was verified by using the video data to measure the thermal growth of the test fixture itself. When compared against the expected growth calculated from the fixture's known CTE, the displacement measurement error was 0.0336 mm, averaged across 20°C - 1000°C. An outlying maximum error of 0.224mm was observed at 824°C, which equates to a expected maximum relative error of 3.60 %, with respect to the curvature and displacement data that will be presented in Section IV.

Finally, we observed an inversion of our video imagery greyscale values at temperatures above roughly 800°C. Essentially, the imagery became a "negative" of its cooler self, which caused the tracking software to fail to lock onto the painted targets. We speculate that this inversion was due to the possibility that our video camera's sensor is sensitive to not just visible light, but also near infra-red (IR) radiation to some degree. Thus, black-painted areas actually appeared brighter than white areas at sufficiently high temperatures, due to a blackbody's greater IR emission intensity. This issue was resolved by using floodlights to drown out the IR emissions with reflected visible light. We also found that consumer-grade digital SLR camera sensors do not seem to be susceptible to this greyscale inversion problem, at least at temperatures less than 1050°C.

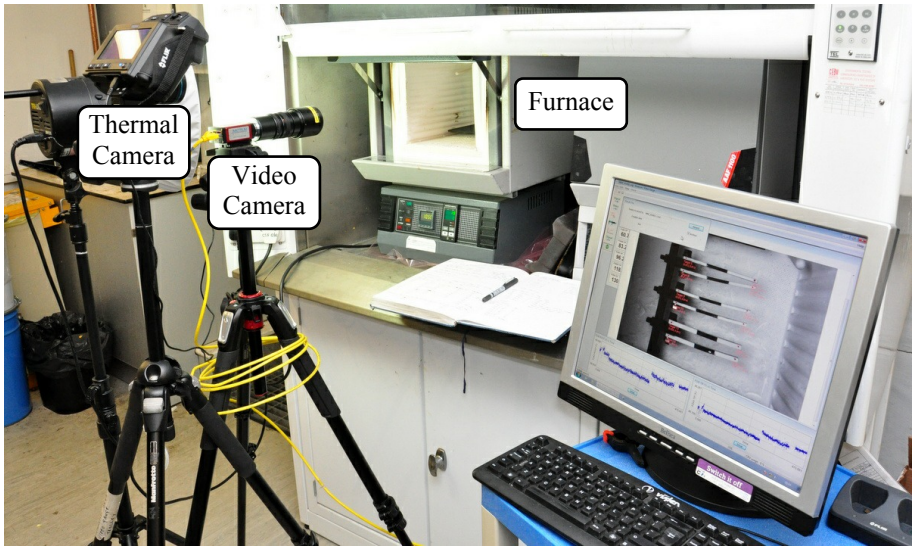

Figure 11. Experimental setup showing optical tracking and thermal cameras positioned in front of furnace.

Temperatures were measured using a FLIR Systems T650sc thermal camera, capturing still images as

depicted in Figure 12. Thermal imaging cameras convert measured radiation intensities to temperatures using an emissivity value set by the user, thus the emissivity of the object to be measured must be known. Heat-resistant black paint was applied to the test fixture so that its emissivity would approximate that of a blackbody emitter, thus enabling the temperature of the fixture to be computed correctly. The actual temperature of each test article was assumed to match that of the fixture at their respective mating surfaces, thus by observing the difference in computed temperature between the fixture and at test article where the two meet, a temperature correction factor could be computed to account for variations in emissivity between test articles.

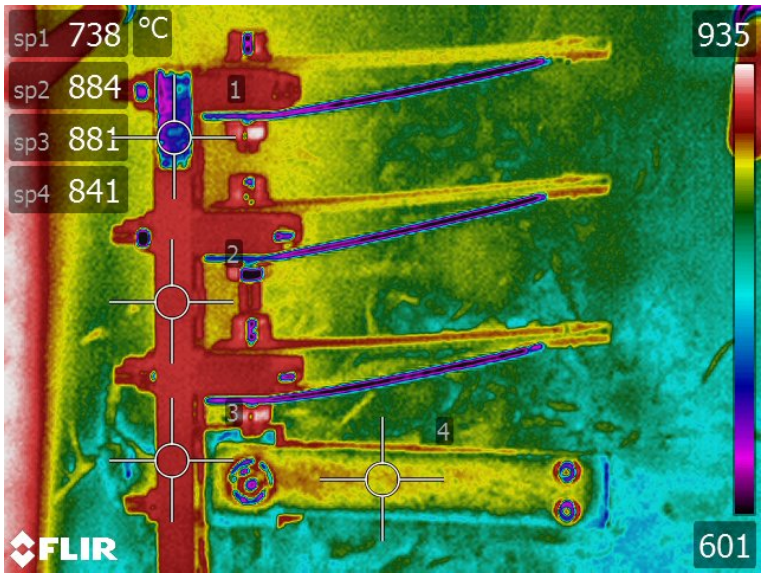

Figure 12. Thermal imagery data showing several CMC-metallic flap section thermal morphing test articles. The regions of markedly lower apparent temperature (T<800°C) are areas where bare metal is exposed, which due to its relatively low emissivity, appears cooler to the thermal camera.

The MMC bimorph test articles were subjected to three heating cycles, with peak temperatures of 394°C, 493°C, and 606°C, respective to each cycle. The CMC-metallic flap-section specimens were subjected to four heating cycles, with peak temperatures of 410°C, 608°C, 824°C, and 1035°C, respective to each cycle.

Curvature of the MMC bimorphs was determined by fitting the relative transverse displacement of the tip target w_{rel} to a circular arc via: $\kappa = \frac{-2w_{\text{rel}}}{L^2+w_{\text{rel}}^2}$, where L is the distance between root and tip targets. Relative displacement was determined by subtracting the root target displacement from the tip target displacement, whereby positive w_{rel} is defined as the $+z$ direction in Figure 10. Assuming curvature across the bimorph is constant, this amounts to defining curvature according to the convention $\kappa = -\partial^2 w/\partial x^2$, thus positive curvature corresponds to a downward curl of the bimorphs as arranged in Figure 10. The targets from which w_{rel} is determined are the black dots shown in Figure 10.

Up to 0.57° of rigid body rotation of the test fixture relative to the video camera was observed throughout the thermal cycling. While it is possible that the fixture experienced a degree of thermally-induced distortion, is is more likely that the bulk of the rotation is due to distortion of the furnace chamber, camera tripod, or even the bench upon which the furnace sat. Regardless, the effect of this rotation was removed by rotating the camera's coordinate data to be square with the test fixture.

As the CMC-metallic flap structures do no display constant curvature along their chord, results are instead presented simply in terms of transverse tip target displacement relative to the root target. As with the MMC bimorphs, rigid body rotation of the test fixture was accounted for in computing displacements.

IV. Results and Discussion

IV.A. MMC-Ti Bimorphs

The thermal response of the MMC-Ti bimorphs is shown in Figure 13, along with curvatures predicted by classical laminate theory (CLT) using the material data in Table 2. Some aspects of these bimorphs' thermal responses make intuitive sense while others do not. We start with a description of the more intuitive features.

On the whole, we can see that the MMC-Ti bimorphs of both 0° and 90° fiber orientation show increasing curvature with increasing temperature. This result is expected, as the MMC layer has a lower CTE than the monolithic titanium layer in both 0° and 90° directions. The curvature rate (i.e. curvature change per unit temperature change) is indicated by the slope of the curves. From this, we can see that curvature develops much faster for 0° fiber orientations vs. 90°, by a factor of about 2.1. This result is also expected, due to the fact that the CTE mismatch between monolithic and composite layers is maximized in the 0° direction.

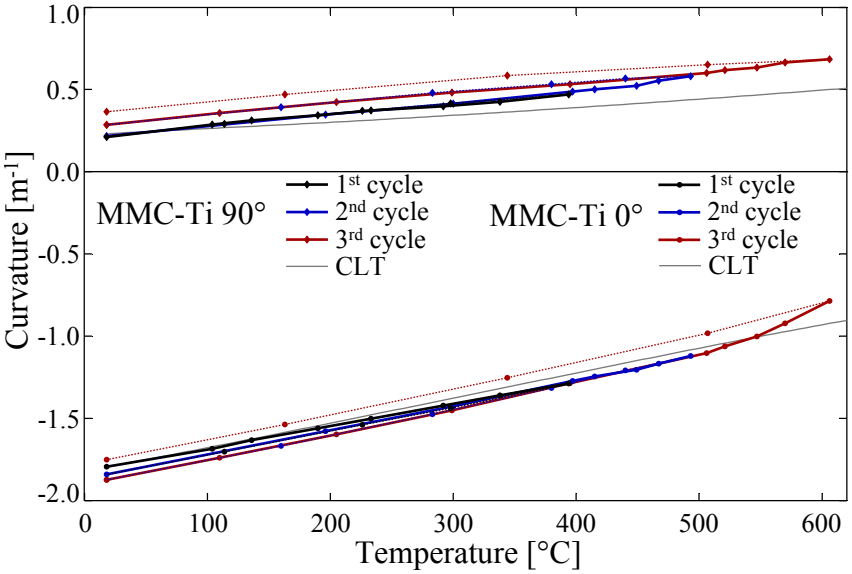

Figure 13. Thermally-induced curvature of MMC-Ti bimorphs.

The first heating cycle reached 394°C, up to which a linear curvature temperature relationship was observed for both 0° and 90° fiber orientations. The second heating cycle reached 493°C. Like the first heating cycle, it also showed a predominately linear temperature-curvature relationship for both fiber orientations. The third heating cycle reached the test's maximum of 606°C. Up to 500°C, the thermal response again was predominately linear, however beyond this temperature, an increase in the rate of curvature generation with respect to temperature was observed for both fiber orientations. This behavior could be due to our titanium alloy's greater CTE at high temperatures, however it is not clear why the nonlinearity is only observed above 500°C, as opposed to across a wider range of temperatures as would be suggested from known CTE data of this material system.

The curvatures observed upon cooling significantly differ from those measured during heating, indicating that some degree of non-recoverable strain has been induced above 500°C. This sort of hysteretic behavior may be expected due to high temperatures yielding or creep effects. Analysis of the internal stress state of the laminate is made complicated by a number of competing factors. Recalling that the laminates were consolidated on a flat tool at approximately 900°C, we expect stresses to increase with departure from this temperature. Thus, we actually expect a reduction in thermally-induced stresses as the bimorphs are heated, so long as the material stays within the elastic regime. However there are two factors which are likely to invalidate this elastic assumption:

1. When cooled from consolidation, the laminate is held restrained against its flat tool by both the isostatic pressure, and the stiffness of the conforming canister in which the laminate is encapsulated. While we cannot say whether the laminate is constrained to a perfectly flat shape during this manufacturing cool-down, it is certainly possible that the stresses induced by this restraint could be of sufficient magnitude to induce yielding in at least one of the layers.

2. The yield stress of Ti-3Al-2.5V is reduced with increasing temperature. At 300°C, for example , the yield stress of this alloy is reduced to 60 % of its room-temperature value.[19] Material data from similar alloys suggests that the reduction in yield stress becomes especially pronounced above 450°C, with results becoming time-dependent as well.[20]

The first item mentioned above would suggest that we would expect yielding to take place at lower tem-

peratures, as that is where thermal stresses are highest. On the other hand, the second item suggests that yielding could also take place at higher temperatures, as that is where the material's yield stress is minimal. Creep could also play a role in contributing to non-recoverable strain. Without a dedicated analysis, it would be quite difficult to determine the exact nature of any non-recoverable strains, however our experimental data does provide us with some clues.

If all strains were elastic, we would expect the bimorphs to recover their flat shape when heated to the consolidation temperature ($\sim$ 900°C). This is clearly not the case for the 90° fiber bimorph. Its room-temperature curvature is positive-signed, which is the opposite of what we would expect based on the sign of the CTE mismatch between layers. The fact that it develops positive curvature with increasing temperature (as expected) allows us to rule out gross errors in our material data, thus the large discrepancy in room-temperature curvature is likely a result of non-recoverable strains developed upon cool-down from consolidation.

In particular, the results are consistent with a scenario whereby the strain developed upon cool-down from consolidation was predominately plastic in the 90° direction, and predominately elastic in the 0° direction. Thus, when the laminate was released from its constraints upon being de-tooled, the stored elastic strain caused the laminate to develop a large degree of curvature in the 0° direction. Meanwhile, the plastic strain in the 90° direction, being non-recoverable, did not contribute to development of curvature in the 90° direction. Instead, the curvature that was developed in the 90° direction was instead *anticlastic curvature*, that is, it was a result of elastic Poisson coupling with the 0° curvature that developed upon detooling.[c] This hypothesis is consistent with the observation that the 90° bimorph's curvatures were offset in the positive direction, relative to the shape that would have been attained from a purely elastic cool-down from consolidation temperature.

In the latter two cycles, the curvature-temperature relationship measured upon heating matched that measured from the previous cooling cycle. This lack of hysteretic behavior at cooler temperatures suggests that the offset in curvatures between successive cycles is due to non-recoverable (e.g. plastic or creep) strains generated at higher temperatures. The coincident temperature-curvature relationship at lower temperatures also suggests that error due to thermal lag between our test specimens and thermal camera measurements is unlikely, otherwise we would see the hysteretic effects at low and high temperatures alike.

By observing trends in the cyclic data, we can draw preliminary conclusions regarding the maximum temperature that can be attained without significant loss of repeatability. These conclusions are somewhat under-conservative, as our test only consisted of three thermal cycles. In other words, it is possible that a temperature-curvature relationship may appear repeatable because two consecutive cycles gave similar results, however there is still the potential for long term drift in the measured curvatures, perhaps due to creep effects, for example.

The 0°-fiber MMC-Ti bimorph showed nearly coincident cyclic data up to 500°C, however the third cycle, which reached 606°C, exhibited non-recoverable deformations as evidenced by the observed hysteresis loop for that cycle. The 90°-fiber specimen, comparatively, showed onset of hysteretic behavior during the second cycle, and thus we cannot consider temperatures above approximately 400°C to give repeatable curvatures for the case of 90° fiber orientation.

IV.B. MMC-304SS Bimorphs

Results for our 0° and 90° fiber orientation MMC-304SS bimorphs are shown in Figure 14 along with CLT analytical predictions. The idea behind using stainless steel as the high-expansion layer is to provide a greater CTE mismatch with the MMC layer compared to using monolithic titanium. A linear fit to the 0° MMC-304SS curvature data gives a curvature rate of $5.4 * 10^{-3}$ $(\mathrm{m} *^{\circ} \mathrm{C})^{-1}$, which represents a 3.6-fold increase in curvature rate over the 0° MMC-Ti bimorph. This factor of curvature rate improvement is nearly identical to the factor by which the CTE mismatch was increased in switching the high-expansion layer from titanium to stainless steel. This result is anticipated by Timoshenko's seminal bimorph model,[6] as well as CLT, which both predict that curvature rate varies in direct proportion to the CTE mismatch between the high and low expansion layers.

Both the 0° and 90° MMC-304SS bimorphs exhibit room temperature curvatures of much lesser magnitude than would be expected if the cool-down from consolidation induced only elastic strains. It is likely that the

[c] In general isotropic plates, unrestrained elastic curvatures are coupled via the relation $\kappa_x = -\nu\kappa_y$. Although our MMC specimens are not isotropic, the same trend applies, in that an elastic change of curvature in one direction leads to an opposite change in the orthogonal direction, albeit scaled down by Poisson's ratio.

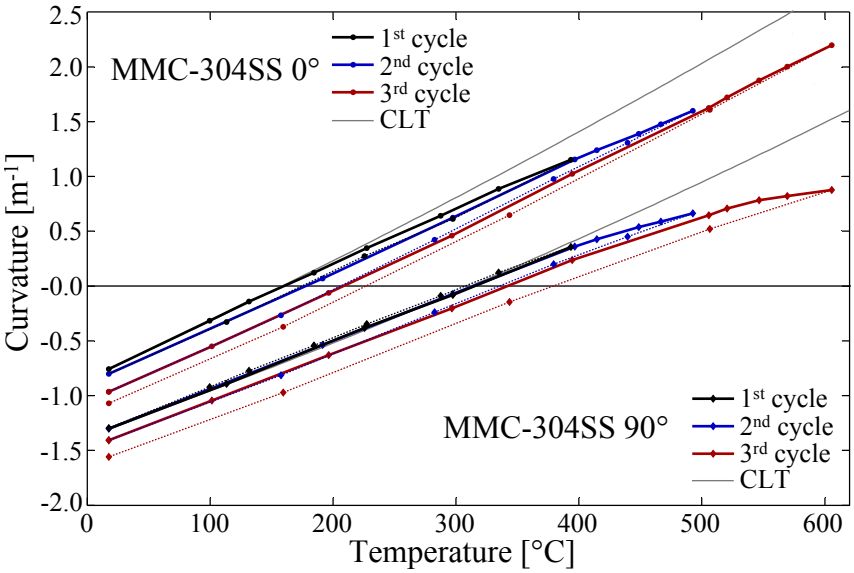

Figure 14. Thermally-induced curvature of MMC-304SS bimorphs.

curvature restraint applied by the HIP process and tooling has induced a significant degree of non-recoverable strain in one or more layers of the laminate. This hypothesis is further supported by the fact that both bimorphs recover a state of zero curvature at temperatures well below their consolidation temperature.

Interestingly, the 0° bimorph's room temperature curvature is offset in the positive direction, though of lesser magnitude, from the 90° bimorph, which is opposite to what was observed with the two MMC-Ti bimorphs. This result is unexpected, as it suggests that upon detooling, the MMC-304SS laminate elastically recovered a lesser magnitude of curvature in the 0° direction relative to the 90° direction. Previous literature indicates that the elastic limit strain of our MMC material is much greater parallel to the fibers vs. perpendicular, which would suggest that we would actually expect a greater degree of elastic curvature recovery in the 0° direction.

Both 0° and 90° bimorphs exhibited a nearly constant curvature rate and small degree of hysteretic behavior during its first thermal cycle. The second cycle showed a decrease in curvature rate above 400°C, and a larger degree of hysteresis upon cooling. The third cycle continued this trend. Notably, the curvatures measured at the peak temperatures of the first and second cycles were nearly identical to the curvatures measured while passing that same temperature during the following cycle. In other words, as each bimorph was heated beyond its previous peak temperature, the curvature "picked up where it had left off" during the previous cycle. This effect is most pronounced in the 90° bimorph, and is reminiscent of the plastic loading, elastic recovery behavior of beams cycled through moments which induce maximum stress beyond their material's elastic limit. It appears that while the use of 304 stainless steel for the high expansion layer does give a great improvement in curvature rate, the additional thermal stresses induced are sufficient to lead to non-recoverable deformations at temperatures greater than about 400°C.

IV.C. CMC-Metallic Flap Section

Results for displacement of the tip tracking target of the CMC-metallic flap section are presented in Figure 15. Also presented are results from a finite element model (ABAQUS 6.12), using 160 S8R shell elements, with geometry and boundary conditions mimicking the experiment. Solutions were obtained using the software's iterative solver in order to account for geometric nonlinearity.

The flap section was put through four temperature cycles, each of progressively higher temperature, up to a maximum of 1035°C. The first cycle to 410°C showed a small degree of nonlinearly in the region of 250-300°C. It is possible that this nonlinearity in the displacement data is due to the CMC and/or 310SS layers slipping slightly at the bolted root joint or riveted tip joint, as there is some clearance between the fastener's outer diameter and holes in the CMC and 310SS layers.

During the second and third thermal cycles, the flap section exhibited a predominately linear displacement-temperature relationship. This is in line with our expectations. The assembly is essentially a pair of beam-

columns, joined at their ends. As long as the axial loads in each beam-column are small relative to the Euler buckling load, we can expect the tip displacement of the assembly to vary approximately in proportion to the growth mismatch of the joined beam-columns. In fact, our finite element (FE) results show that with sufficient growth mismatch (i.e., sufficient ΔT), the compression member buckles in the Euler manner, and further increases in tip displacement are greatly restricted thereafter. For the current geometry, this buckling is not forecast to occur until well beyond the tested temperature range. However, note that this buckling action is sensitive to geometry. Naturally, flap sections of long chord and low thickness are more susceptible to buckling than those of stouter proportions for a given pair of skin materials. We also make note that other workers have successfully addressed the buckling problem by joining the high and low-expansion skins with spanwise ribs, thus allowing the skin in compression to be supported by the adjacent, tension-stabilized skin.[12]

The fourth thermal cycle also showed a predominately linear temperature-displacement relationship, however the displacement values were offset to lower values from the previous cycles. Bearing in mind that the assembly was joined in a stress-free state at room temperature, we can hypothesize that this non-elastic behavior was a result of the higher stresses at elevated temperatures, thermal degradation of material properties, or some combination thereof. There is of course the additional possibility that slip in the bolted or riveted joints is at least partly responsible, however our displacement measurement method does not allow us to separately analyze these potential sources of nonlinearity.

It is difficult to evaluate the maximum temperature that gives repeatable deformations. While the second and third cycles showed some degree of hysteretic behavior, the fourth cycle exhibited almost completely recoverable deformation. This unexpected trend in our results lends more weight to the possibility that the prior cycle's non-recoverable deformations were due to slip in the joints.

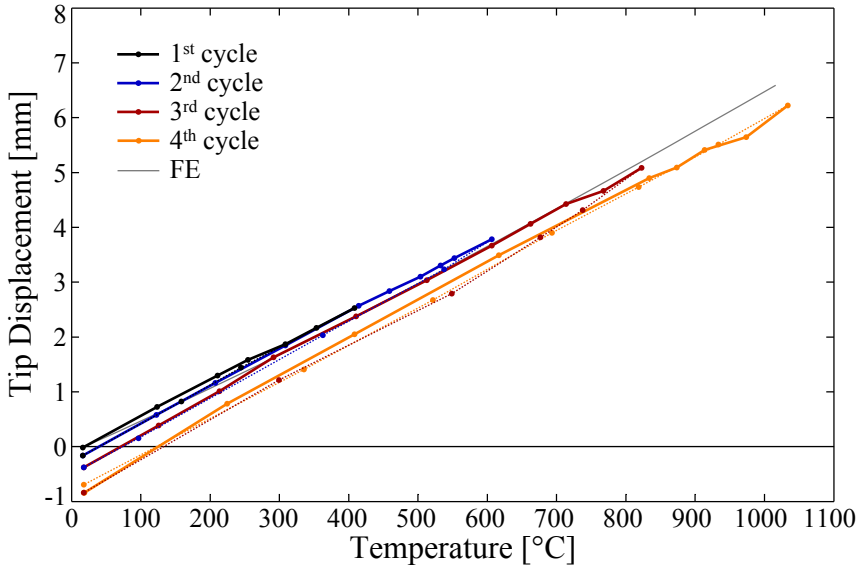

Figure 15. Experimentally-measured and finite element (FE) results showing the thermally-induced tip displacement of CMC-metallic flap section.

Figure 16 shows an image of the flap section near the maximum test temperature superimposed upon its room temperature shape. Note that the 310SS skin, which acts in compression, has a higher degree of curvature along its length than the tension-stabilized C/SiC skin, as we would expect based on a joined beam-column representation of the structure.

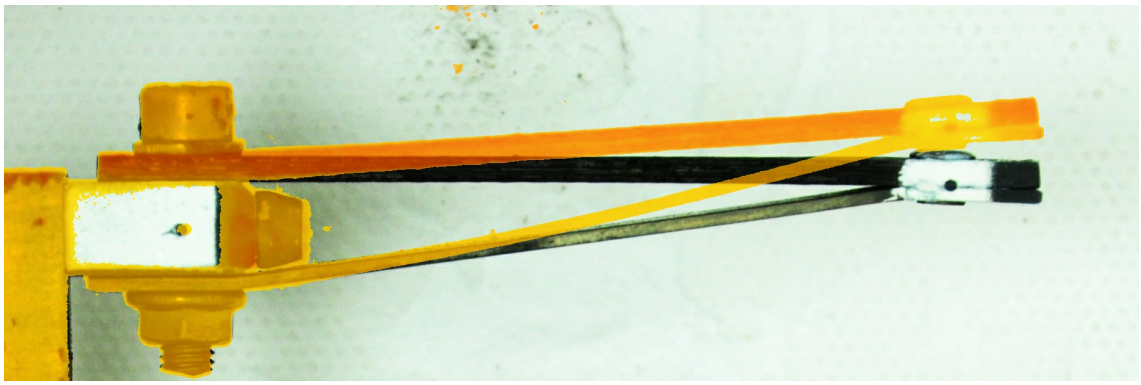

Figure 16. Image of the CMC-metallic flap section at $\sim 1000^{\circ}$C in its naturally-occurring orange glow, overlaid upon an image of the same structure at room temperature.

V. Conclusions

Three concepts for achieving thermally-driven morphing at high temperatures were developed and demonstrated in a furnace environment. An optical displacement measurement approach proved satisfactory for the needs of the experiment, however issues with our camera's sensitivity to IR radiation had to be overcome.

MMC-Ti bimorphs exhibited a repeatable curvature response to thermal loading at temperatures up to 500°C in the fiber direction, and up to 400°C perpendicular to the fibers. Long term cyclic testing was not carried out, thus these temperature values could be under-conservative for long-exposure or highly cyclic applications. The rate of curvature development was 2.1 times faster in the fiber direction versus perpendicular, a reflection of the low longitudinal CTE of the SiC fibers relative to the titanium matrix. Manufacturing-induced strains occurring during cool-down in a closed tool were primarily elastic in the fiber direction, and predominately plastic the perpendicular direction.

MMC-304SS construction improved the CTE mismatch between layers by a factor 3.6 relative to MMC-Ti construction, along the fiber direction. This increase translated into an equivalent factor of improvement in the rate of curvature development with respect to temperature, a result predicted by Timoshenko's bimorph model and CLT alike.

MMC-304SS bimorphs failed to recover their room temperature curvatures when heated beyond 400°, however upon further cycling, the curvature-temperature relationship remained linear at up to 600°C in the fiber direction, and up to 500° in the perpendicular direction. This behavior, which resembles cycling strain hardening, is likely instead due to a redistribution of residual stresses within the laminate which occurs, for example, in beams stressed passed their elastic limit. This leads to a scenario whereby the first cycle to a particular temperature may show elastic-plastic behavior, however further cycles to this same temperature show only elastic behavior. The manufacturing process induced non-elastic strains in both the fiber and perpendicular directions.

We attempted to create a CMC-metallic bimorph from in-house manufactured C/SiC CMC, brazed to Inconel 625. While successful joints could be created for small coupon-sized specimens, larger laminates debonded at the CMC-braze interface.

The large CTE mismatch between CMCs and heat resisting alloys can still be exploited through use of alternate geometries. A mechanically-joined flap-section arrangement was studied, and a section of 80 mm chord was found to produce a tip displacement of 7 mm at 1035°C. The tip displacement was found to be generally linearly proportional to temperature change, however the original geometry was not recovered exactly upon completion of thermal cycling. This permanent deformation may be due to yield or creep within the skins, or slip between the skins at their bolted and riveted interfaces. One advantage accorded by a mechanical fastening strategy is the fact that the assembly is essentially stress-free at room temperature. This feature could simplify structural analysis compared to, for example, the MMC-based bimorphs which develop significant residual stresses during the course of their manufacturing.

It is envisioned that thermally-driven morphing structures will allow the advantages of adaptive structures to be exploited in environments previously considered too hot, or otherwise hostile to existing actuation and motion systems.

Acknowledgments

The authors would like to thank Peter Martin and Ian Gent for their invaluable SEM and EDX analysis efforts, Dr. Mrityunjay Singh for his many helpful comments and guidance regarding CMC-metallic structures, and the personnel at TISICS Inc. for their advice regarding the design and manufacturing of metal matrix composites. This effort was sponsored by the European Office of Air Force Research and Development, Air Force Office of Scientific Research, USAF, under grant number FA9550-14-1-0063. The U.S. Government is authorized to reproduce and distribute reprints for governmental purpose notwithstanding any copyright notation thereon. The views and conclusions contained herein are those of the authors and should not be interpreted as necessarily representing the official policies or endorsements, either expressed or implied, of the Air Force Office of Scientific Research or the U.S. Government. This work was also supported by the Engineering and Physical Sciences Research Council through the EPSRC Centre for Doctoral Training in Advanced Composites for Innovation and Science, grant number EP/G036772/1.

References

[1]Culley, D., Garg, S., Hiller, S. J., Horn, W., Kumar, A., Mathews, H. K., Moustapha, H., Pfoertner, H., Rosenfeld, T., Rybarik, P., Schadow, K., Stiharu, I., Viassolo, D. E., and Webster, J., "More Intelligent Gas Turbine Engines," Tech. Rep. RTO-TR-AVT-128, NATO RTO, April 2009.

[2]Mercer, C. R., Haller, W. J., and Tong, M. T., "Adaptive Engine Technologies for Aviation CO2 Emissions Reduction," Tech. Rep. NASA/TM-2006-214392, Aug. 2006.

[3]Lattime, S. B. and Steinetz, B. M., "High-pressure-turbine clearance control systems: current practices and future directions," *Journal of Propulsion and Power*, Vol. 20, No. 2, 2004, pp. 302–311.

[4]Huber, J. E., Fleck, N. A., and Ashby, M. F., "The selection of mechanical actuators based on performance indices," *Proceedings of the Royal Society of London. Series A: Mathematical, Physical and Engineering Sciences*, Vol. 453, No. 1965, Oct. 1997, pp. 2185–2205.

[5]Sobel, D., *Longitude: The True Story of a Lone Genius Who Solved the Greatest Scientific Problem of His Time*, Walker & Company, Oct. 2007.

[6]Timoshenko, S., "Analysis of bi-metal thermostats," *J. Opt. Soc. Am*, Vol. 11, No. 3, 1925.

[7]Chang, M. H. and Mancuso, R., "A compilation of design and performance characteristics for thermal louver systems," *19th Thermophysics Conference*, American Institute of Aeronautics and Astronautics, June 1984.

[8]Wittrick, W. H., Myers, D. M., and Blunden, W. R., "Stability of a Bimetallic Disk," *The Quarterly Journal of Mechanics and Applied Mathematics*, Vol. 6, No. 1, March 1953, pp. 15–31.

[9]Mansfield, E. H., "Bending, Buckling and Curling of a Heated Elliptical Plate," *Proceedings of the Royal Society of London. Series A. Mathematical and Physical Sciences*, Vol. 288, No. 1414, Nov. 1965, pp. 396–417.

[10]Asanuma, H., Haga, O., and Imori, M., "Development of High Performance CFRP/Metal Active Laminates," *JSME International Journal Series A Solid Mechanics and Material Engineering*, Vol. 49, No. 1, 2006, pp. 32–37.

[11]Asanuma, H., Hakoda, G., and Mochizuki, T., "Fabrication of Nickel Based Active Composites," *JSME International Journal Series A Solid Mechanics and Material Engineering*, Vol. 46, No. 3, 2003, pp. 473–477.

[12]Chau, E., *A Comparative study of Joining Methods for a SMART Aerospace Application*, Ph.D. thesis, Cranfield University School of Applied Sciences, April 2007.

[13]Feillard, P., "The high temperature behaviour of long fibre reinforced titanium under transverse loading," *Acta Materialia*, Vol. 44, No. 2, Feb. 1996, pp. 643–656.

[14]Hess, M. S., "The End Problem for a Laminated Elastic Strip: II Differential Expansion Stresses," *Journal of Composite Materials*, Vol. 3, No. 4, Oct. 1969, pp. 630–641.

[15]Ghosh, S. K. and Chatterjee, S., "On the Direct Diffusion Bonding of Titanium Alloy to Stainless Steel," *Materials and Manufacturing Processes*, Vol. 25, No. 11, 2010, pp. 1317–1323.

[16]Kundu, S., Ghosh, M., Laik, A., Bhanumurthy, K., Kale, G. B., and Chatterjee, S., "Diffusion bonding of commercially pure titanium to 304 stainless steel using copper interlayer," *Materials Science and Engineering: A*, Vol. 407, No. 1, Oct. 2005, pp. 154–160.

[17]Robertson, J. G., "Manufacture and Properties of Sigma Fibre Reinforced Titanium," Tech. Rep. AGARD-R-796, NATO Advisory Group for Aerospace Reserach and Development, Feb. 1994.

[18]Thomas, M. P. and Winstone, M. R., "Effect of the angle between fibres and tensile axis on static properties of unidirectional reinforced titanium MMC," June 1998.

[19]Welsch, G., Boyer, R., and Collings, E. W., *Materials Properties Handbook: Titanium Alloys*, ASM International, Dec. 1993.

[20]*ESDU Metallic Materials Data Handbook*, Supplement 47, IHS ESDU, July 2012.

[21]Committee, A. H., *Metals Handbook*, American Society for Metals, 9th ed., 1980.

[22]Krenkel, W., editor, *Ceramic Matrix Composites: Fiber Reinforced Ceramics and Their Applications*, Wiley VCH, Weinheim, 1st ed., May 2008.

[23]Hurwitz, F. I., "Filler/Polycarbosilane Systems as CMC Matrix Precursors," *Ceramic Engineering and Science Proceedings*, Vol. 19, 2008, pp. 267 – 274.

[24]Jian, K., Chen, Z.-H., Ma, Q.-S., Hu, H.-F., and Zheng, W.-W., "Processing and properties of 2D-Cf/SiC composites incorporating SiC fillers," *Materials Science and Engineering: A*, Vol. 408, No. 1, Nov. 2005, pp. 330–335.

[25]Hsueh, C. H. and Evans, A. G., "Residual Stresses in Meta/Ceramic Bonded Strips," *Journal of the American Ceramic Society*, Vol. 68, No. 5, May 1985, pp. 241–248.

[26]Singh, M., Shpargel, T., Morscher, G. N., Halbig, M. H., and Asthana, R., "Robust Joining and Integration Technologies for Advanced Metallic, Ceramic, and Composite Systems," Cocoa Beach, FL, United States, Jan. 2006.